Athermal Resistance to Interface Motion in the Phase-Field Theory of Microstructure Evolution

Valery I. Levitas and Dong-Wook Lee
Department of Mechanical Engineering, Texas Tech University, Lubbock, Texas 79409, USA
(Received 9 March 2007; published 10 December 2007)

A method of introducing an athermal resistance to interface propagation for the Ginzburg-Landau (GL) approach to the first-order phase transformations (PTs) is developed. It consists of introducing oscillating fields of stresses (due to various defects or a Peierls barrier) or a jump in chemical energy. It removes some essential drawbacks in GL modeling: it arrests experimentally observed microstructures that otherwise converge to a single phase, and it reproduces rate-independent stress hysteresis. A similar approach can be applied for twinning, dislocations, and other PTs (e.g., electric and magnetic).

DOI: 10.1103/PhysRevLett.99.245701 PACS numbers: 64.70.K−, 64.60.−i, 81.30.Kf

The phase-field or Ginzburg-Landau (GL) equations are employed for the description of a wide class of first-order phase transformations (PTs), including martensitic, reconstructive, ferroelectric, ferroelastic, and magnetoelastic PTs. They also describe dislocation motion and twinning. Despite significant success in modeling the microstructure formation [1–7], the GL approach has a major drawback: it neglects an athermal resistance to interface motion. To be specific, we will focus on the temperature- and stress-induced martensitic PTs between austenite (A) and i martensitic variants (M_i). Athermal friction K is caused by the Peierls barrier as well as by the interaction of the moving interface with long-range stress fields of various defects (such as point and linear defects and various boundaries) [8]. The driving force for PT has to exceed K in order for the interface to propagate, and the athermal resistance is responsible for the rate-independent part of the stress or temperature hysteresis and energy dissipation. We found in our numerous simulations of a single crystal, and for the homogeneous stresses at the boundary, that nonstationary solutions pass through some complex martensitic microstructures that resemble those observed experimentally; however, they finally converge to a single phase (see also [5]). This does not allow us to model experiments with stress-free surfaces (temperature-induced PT) or with homogeneous stresses at the boundaries. Even for periodic boundary conditions, in some cases a single variant was obtained as well [1,6]. When kinematic constraints—due to prescribed displacements, polycrystalline sample, or thin film on a substrate—are imposed, multivariant stationary microstructure is observed [1,4,5]. However, allowing for an athermal threshold, which exists in any case, would change the microstructure evolution, energetics, and path dependence.

An athermal threshold is included in all mesoscale models [8,9] that deal with the kinetic equation for sharp interface or concentration of a product phase. However, introduction of the athermal threshold is not a straightforward problem for the GL approach because it does not use an equation for the interface. For example, introducing a threshold in the kinetic equation for the order parameters arrests some nonphysical intermediate configurations obtained in the dynamic process, in particular, critical nuclei. While the necessity to introduce an athermal threshold has been recognized for a long time, we are not aware of any solution to this problem.

In this Letter, we suggest and study a method for including the athermal threshold in the GL approach. We show that introduction of spatially oscillating fields of stresses (due to the Peierls barrier and various defects) or of a jump in chemical energy ΔG^θ reproduces the effect of the athermal threshold and the rate-independent hysteresis. These fields do not arrest an intermediate microstructure. Also, these fields reproduce some microstructures observed experimentally that would not follow from the GL energy minimization. A similar approach can be applied for other PTs, as well as for dislocation motion.

Model.—Recently [10], a 3D Landau theory for stress-induced martensitic PTs was developed. It can describe all temperature-dependent thermomechanical properties of the A and M phases and PTs between A and M_i and between M_i for any type of their symmetry, as well as typical stress-strain curves. We will use the Gibbs energy G and the transformation strain tensor $\boldsymbol{\varepsilon}_t$ in the form [10]

$$G = -\frac{1}{2}\boldsymbol{\sigma}:\boldsymbol{\lambda}:\boldsymbol{\sigma} - \boldsymbol{\sigma}:\boldsymbol{\varepsilon}_t + \sum_{k=1}^{n} f(\theta, \eta_k) + \sum_{i=1}^{n-1}\sum_{j=i+1}^{n} F_{ij}(\eta_i, \eta_j), \tag{1}$$

$$\boldsymbol{\varepsilon}_t = \sum_{k=1}^{n} \boldsymbol{\varepsilon}_t^k [a\eta_k^2 + (4-2a)\eta_k^3 + (a-3)\eta_k^4], \tag{2}$$

with

$$f(\eta_k) = A\eta_k^2 + (4\Delta G^\theta - 2A)\eta_k^3 + (A - 3\Delta G^\theta)\eta_k^4,$$

$$F_{ij}(\eta_i, \eta_j) = B\eta_i\eta_j(1-\eta_i-\eta_j)\{B[(\eta_i-\eta_j)^2 - \eta_i - \eta_j] + D\eta_i\eta_j\} + \eta_i^2\eta_j^2(\eta_i Z_{ij} + \eta_j Z_{ji}),$$

and

$$Z_{ij} = \bar{A} - A + \boldsymbol{\sigma}:[(a-3)\boldsymbol{\varepsilon}_t^j + 3\boldsymbol{\varepsilon}_t^j].$$

Here, $\boldsymbol{\sigma}$ is the stress tensor; θ is the temperature; η_i and $\boldsymbol{\varepsilon}_j^i$ are the order parameter and the transformation strain tensor of the ith variant, respectively; $i = 0$ corresponds to A; $\boldsymbol{\varepsilon}_t^0 = 0$; $\boldsymbol{\lambda}$ is the elastic compliance tensor; and A $\bar{A}$, B, and C are parameters. In the calculations, we use material parameters for cubic to tetragonal PT in NiAl found in [10]. The GL energy

$$G_{\mathrm{GL}} = G + \beta \sum_{k=1}^{n} (\nabla \eta_k)^2$$

leads to the n time-dependent GL equations

$$\frac{\partial \eta_k}{\partial t} = 2\lambda\beta\nabla^2\eta_k - \lambda\frac{\partial G}{\partial \eta_k}, \tag{3}$$

where β is the gradient energy coefficient and ∇ is the gradient operator. This also leads to the elasticity law that has to be supplemented by the equilibrium equations and the relationship between strains and displacements $\boldsymbol{u}$:

$$\boldsymbol{\sigma} = \boldsymbol{\lambda}^{-1}:(\boldsymbol{\varepsilon} - \boldsymbol{\varepsilon}_t) + \boldsymbol{\sigma}_d; \quad \nabla\cdot\boldsymbol{\sigma} = 0; \quad \boldsymbol{\varepsilon} = (\nabla \boldsymbol{u})_s, \tag{4}$$

where $\boldsymbol{\sigma}_d$ is the oscillating stress field of defects and $()_s$ means symmetrization. The structure of Eqs. (3) and (4) is similar to the structure of coupled thermoelasticity. Equation (3) resembles the thermal conductivity equations for n temperatures η_k and stress-dependent heat sources $\lambda\partial G/\partial\eta_k$. The thermal strain corresponds to $\boldsymbol{\varepsilon}_t$ with a complicated temperature dependence (2). The found similarity has important computational consequences: it allows modifying a finite element thermoelasticity code for phase-field modeling of PTs. In this work, we used the code FEAP [11]. We consider square sample of size $l =$ 60 nm under plane strain conditions, $\theta = 100$ K, and at the boundaries constant stresses $\boldsymbol{\sigma}_b = (\sigma_{1b}, \sigma_{2b})$ are applied and $\boldsymbol{n}\cdot\nabla\eta_k = 0$, where $\boldsymbol{n}$ is the normal to the boundary. For 2D problems only 2 M_i are considered with the components of $\varepsilon_{tk}^1 = (0.215; -0.078; -0.078)$ and $\varepsilon_{tk}^2 = (-0.078; 0.215; -0.078)$.

Prescription of oscillating fields.—Usually, kinetic equations for thermally activated dislocation or interface motion are derived by considering some spatially oscillating energy profile that mimics the Peierls barrier and the energy profiles of various defects [8]. We will introduce an oscillating in space energy profile through oscillating stress fields of some defects (e.g., $\boldsymbol{\sigma}_d = K\boldsymbol{\varepsilon}_{t1}\sin(2\pi x/b)/(\boldsymbol{\varepsilon}_{t1}:\boldsymbol{\varepsilon}_{t1})$) or through the oscillating contribution to ΔG^θ. The period b is determined by the actual field of defects; e.g., b is the period of crystal lattice for the Peierls barrier. Then the Landau potential for $\eta_1 = 1$ contains an additional transformation work, $K\sin(2\pi x/b)$, which produces an effect similar to the interface friction K. A similar effect can be obtained by adding $K\sin(2\pi x/b)$ to ΔG^θ. For $\boldsymbol{\sigma}_d = (\sigma_{1d}, \sigma_{2d})$, the thermodynamic driving force for $M_1 \rightarrow M_2$ PT due to the stress fields of defects is $X_{1\to2}^d = \boldsymbol{\sigma}_b:(\boldsymbol{\varepsilon}_t^2 - \boldsymbol{\varepsilon}_t^1) = 0.293(\sigma_{2d} - \sigma_{1d})$. The similar driving force due to boundary conditions is $X_{1\to2}^b = \boldsymbol{\sigma}_b:(\boldsymbol{\varepsilon}_t^2 - \boldsymbol{\varepsilon}_t^1) = 0.293(\sigma_{2b} - \sigma_{1b})$. Now, let us consider 2D examples.

(1) The initial conditions are randomly distributed η_i fields, and the boundary conditions are $\sigma_{ib} = 10$ GPa, i.e., $X_{1\to2}^b = 0$. The solutions of Eqs. (1)–(4) converge (through quite complex microstructure, containing plates, laths, and needles) to $M_1 - M_2$ twins [Figs. 1(a) and 1(b)] and then to M_1 or M_2. The stationary solution to the same problem but with $\sigma_{2d}(H) := H\sin(16\pi x)\sin(16\pi y) = -\sigma_{1d}$ [and consequently $X_{1\to2}^d = 0.586\sigma_{2d}(H)$, as shown in Fig. 1(c)] and with $H = 10$ GPa, is shown in Fig. 1(d). In the absence of surface energy and internal stresses due to transformation strain, a minimum of the energy would correspond to microstructures with M_1 (M_2) in the regions with $X_{1\to2}^d < 0$ ($X_{1\to2}^d > 0$). Elastic energy due to evolving transformation strain fields promotes the appearance of straight plates aligned under 45° [Fig. 1(d)], and the surface energy promotes coalescence. The field $X_{1\to2}^d$ affects the initial stages of formation of the microstructure, reducing the size of initial M_i units according to their period. In this stage, elastic and surface energy exceed the potential barriers due to the $X_{1\to2}^d$ field, and the units coalesce. When the system converges to the twin microstructure in Fig. 1(d), it is arrested; some portions of plates are stuck in the regions where $X_{1\to2}^d$ suppresses them. Small islands within broad M_2 plates in Fig. 1(d) represent a not completely transformed variant stabilized by the field $X_{1\to2}^d$ of defects. In case of reduction of σ_{2b}, and consequently $X_{1\to2}^b$, these islands will serve as heterogeneous nucleation sites due to defects for M_1. The fields $\sigma_{1d} = 5\cos(16\pi x)\cos(16\pi y)$

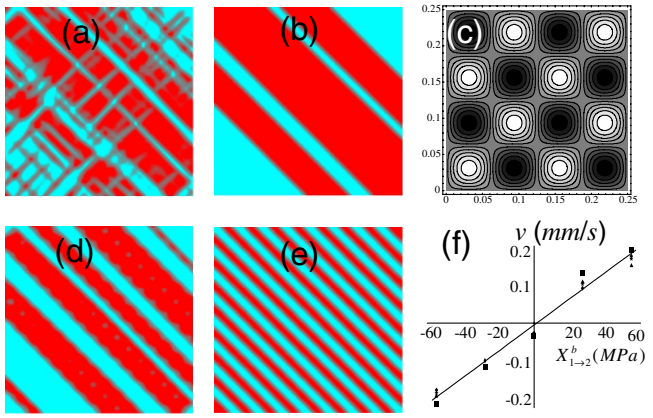

FIG. 1 (color online). Evolution of randomly distributed η_i fields for $\sigma_{ib} = 10$ GPa. (a) and (b) Without a defects field, which finally converges to M_2. (c) Distribution of the stresses of defects $\sigma_{2d} = 10\sin(16\pi x)\sin(16\pi y) = -\sigma_{1d}$ and the driving force $X_{1\to2}^d = 0.586\sigma_{2d}$ in a quarter of the sample; in black (white) regions variant M_2 (M_1) is promoted. (d) Corresponding stationary microstructure. (e) Stationary microstructure for $\sigma_{1d} = 5\cos(16\pi x)\cos(16\pi y)$ and $\sigma_{2d} = 5\sin(16\pi x)\times\sin(16\pi y)$ and consequently $X_{1\to2}^d = -1.465\cos[16\pi(x+y)]$ (periodic function along the diagonal); everywhere blue (light gray) is M_1 and red (dark gray) is M_2. (f) Plot interface velocity v vs the macroscopic driving force $X_{1\to2}^b$ for four interfaces from microstructure in (e).

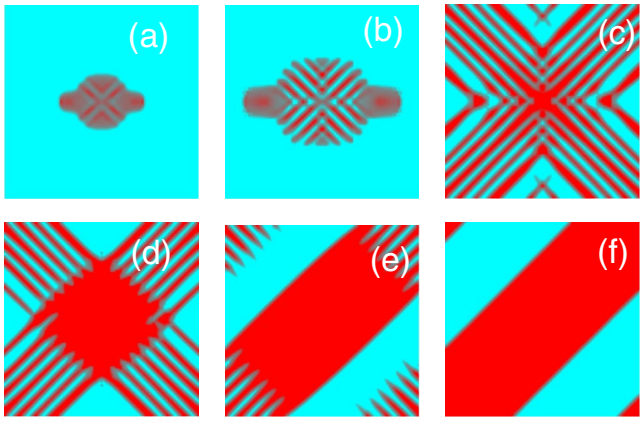

FIG. 2 (color online). Evolution of initial embryo $\eta_i = 0.1$ in a circle of the radius of 2 nm at the center of the sample for $\sigma_{ib} = 15$ GPa; stationary microstructure is M_2. (a) and (b): Blue (light gray) outside of M_2 units is A and red (dark gray) is M_2; distribution for M_1 is rotated by 90° distribution for M_2. (c)–(f): Blue (light gray) is M_1 and red (dark gray) is M_2.

and $\sigma_{2d}(5)$ lead to completely different $X^d_{1\to2} = -1.465\cos[16\pi(x+y)]$—i.e., to a periodic function along the diagonal. The initial microstructures coalesce into an alternating, equally sized $M_1 - M_2$ microstructure oriented under 45° [Fig. 1(e)].

(2) The stationary microstructure obtained in the previous problem [Fig. 1(e)] was taken as an initial condition, with $\sigma_{ib} = 10$ GPa. When the σ_{id} were removed, the M_1 plates started to widen until the transformation to M_1, driven by the reduction of surface energy, was complete. When, prior to PT completion, σ_{1b} was decreased (e.g., to 9.9 GPa), a complete reverse PT $M_1 \rightarrow M_2$ was observed. Plot interface velocity v vs the macroscopic driving force $X^b_{1\to2}$ for four interfaces is presented in Fig. 1(f). The small, nonzero velocity for $X^b_{1\to2} = 0$ is caused by the driving force due to the reduction of surface energy. For an interface of constant length, $v = 0$ for $X^b_{1\to2} = 0$, which is also confirmed by our 1D analytical solution.

To introduce an athermal hysteresis, we studied a stepwise stress field $\sigma_{2d} = -\sigma_{1d} = \pm\mathrm{H} = \pm 2$ GPa (i.e., $X^d_{1\to2} = \pm 0.586$ H) in bands inclined under 45° with the width of $b = 0.2l$. Stochastic initial data under $\sigma_{ib} = 10$ GPa converges to the twinned microstructure, the configuration of which coincides with the region of positive and negative $X^d_{1\to2}$. Keeping $\sigma_{2b} = 10$ GPa, for $6 < \sigma_{1b} < 14$ GPa, interfaces do not move, as expected. Only for $\sigma_{1b} > 14$ GPa ($\sigma_{1b} < 6$ GPa) does the variant M_1 (M_2) grow until PT is complete. When we used $\sigma_{1d} = 5\cos(6\pi x)\cos(6\pi y)$ and $\sigma_{2d} = 5\sin(6\pi x)\sin(6\pi y)$ (i.e., $X^d_{1\to2} = -1.465\cos[6\pi(x+y)]$) and $\sigma_{ib} = 10$ GPa, we obtained the same stationary structure as for the stepwise fields. However, when we varied σ_{1b} between 5 and 15 GPa, the concentration and width of all stationary twins varied continuously and coalesced to pure M_2 (M_1) at 5 GPa (15 GPa). Thus, there is an expected deviation of transformation stresses from thermodynamically equilibrium ones. However, the stress versus twin concentration curve under slow cyclic loading does not exhibit a hysteresis loop and energy dissipation.

(3) Initial conditions are $\eta_i = 0.1$ in the circle of the radius of 2 nm at the center of the sample; $\sigma_{ib} = 15$ GPa. A complicated microstructure consisting of a combination of four herringbone types of microstructure is developed (Fig. 2) and evolves into a twinned microstructure and finally to M_1. Adding $\sigma_{1d} = 5\cos(16\pi x) \times \cos(16\pi y)$ and $\sigma_{2d}(5)$ completely changes the evolution to the stationary structure with the equal width of twins, where M_2 (M_1) is located in the region with positive (negative) $X^d_{1\to2} = -1.465\cos[16\pi(x+y)]$ [Fig. 1(e)]. For $\sigma_{1d} = H\sin[16\pi(x)]\sin(16\pi y) = -\sigma_{2d}(H)$ ($X^d_{1\to2} = 0.586\sigma_{2d}(H)$, see Fig. 1(c), and $H = 10$ GPa, $X^d_{1\to2}$ drives the microstructure to four twinned regions with clear boundaries (Fig. 3). There is a remarkable change in neighbors: many M_1 variants from one grain contact M_2 variants from other grains. However, the energy of internal stresses and surface energy exceed the barriers due to $X^d_{1\to2}$. Coalescence of M_1 starts along the paths with relatively low $X^d_{1\to2}$, M_1 surrounds regions with maximum of $X^d_{1\to2}$, and the final stationary solution is a two-twin microstructure, even for $H = 20$ GPa [Fig. 3(d)]. When we used stepwise $\sigma_{2d} = -\sigma_{1d}$, and consequently $X^d_{1\to2} = 0.589\sigma_{2d}$ as shown in Fig. 4(a), the resultant four-grain microstructure was arrested [Fig. 4(c)].

(4) For the same initial and boundary conditions, we used stepwise $\sigma_{2d} = -\sigma_{1d}$, and consequently $X^d_{1\to2} = 0.589\sigma_{2d}$ as shown in Fig. 5(a); the width of each step is $b = 0.2l$. The stationary microstructure con-

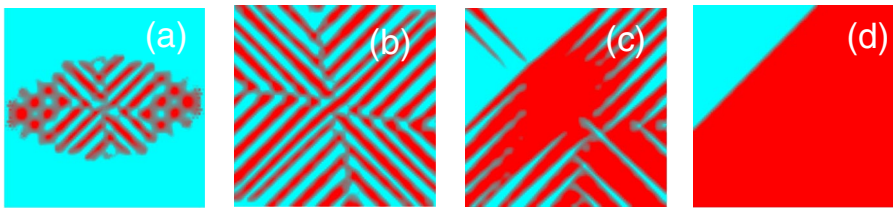

FIG. 3 (color online). The same problem as in Fig. 2 but with $\sigma_{2d} = 10\sin(16\pi x)\sin(16\pi y) = -\sigma_{1d}$, i.e., with $X^d_{1\to2} = 0.586\sigma_{2d}$ from Fig. 1(c). (a) Blue (light gray) outside of M_2 units is A and red (dark gray) is M_2. (b)–(d): Blue (light gray) is M_1 and red (dark gray) is M_2. (d) is the stationary microstructure.

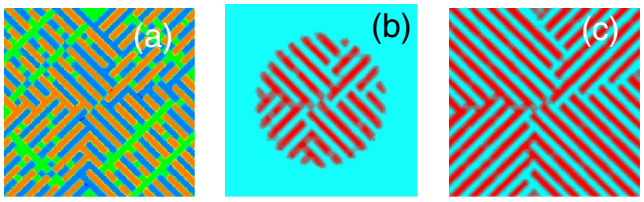

FIG. 4 (color online). Similar problem as in Fig. 2 but with $\sigma_{2d} = -\sigma_{1d}$ and $X^d_{1\to 2} = 0.586\sigma_{2d}$ shown in (a). Stress values are -10 (yellow, light gray), 0 (green, intermediate gray), and 10 GPa (blue, dark gray). (b) and (c) are the intermediate and stationary microstructures.

sists mostly of laths of rectangular shape and a few needle-like units [Fig. 5(c)]. Lath microstructure is observed when PT is accompanied by dislocation generation [8]. Without an athermal threshold, such a structure cannot be obtained because minimization of elastic energy leads to relatively sharp tips.

(5) For the similar problem with $\sigma_{2d} = -\sigma_{1d}$, and consequently $X^d_{1\to 2} = 0.589\sigma_{2d}$ (with $b = 0.1l$) shown in Fig. 5(d), the microstructure evolves like at the initial stage of microstructure evolution without defects [Fig. 2(c)]; however, the defects field arrests it [12].

To summarize, we suggested introducing oscillating fields of stresses due to defects or ΔG^θ to model an athermal threshold in the GL equation. With these fields, experimentally observed microstructures are self-arrested before converging to a single phase, and rate-independent stress and temperature hysteresis are reproduced. In addition to producing an athermal threshold, these fields also create sites for heterogeneous nucleation. Oscillating fields not only open new opportunities for realistic microstructure modeling but also lead to a new problem: how to find a realistic oscillating field corresponding to the given defect structure. For any given (experimentally observed) distribution of dislocations and other defects, we can find a numerically corresponding stress field $\boldsymbol{\sigma}^d$ using, e.g., the approach in [3]. For any given (or evolving) heterogeneous alloy composition, in cases in which the dependence of ΔG^θ on composition is known and included in the simulation, the heterogeneous (oscillating) contribution to ΔG^θ appears automatically. The effect of the stress field of defects can be characterized by the field of the driving force $X^d_{1\to 2}$ that gives some idea about the possible effect of $\boldsymbol{\sigma}^d$ on the microstructure evolution. However, because the two traditional contributions to the driving force—the surface energy and the energy of internal stresses due to $\boldsymbol{\varepsilon}_t$—depend upon the evolving geometry of M_2, the final microstructure may be very sensitive to the change in $X^d_{1\to 2}$.

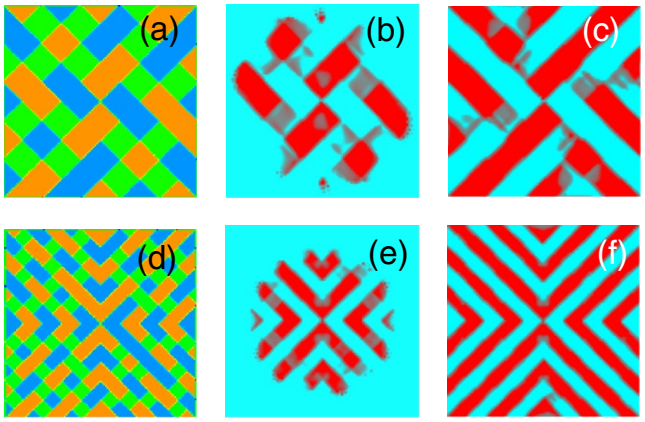

FIG. 5 (color online). Two similar problems as in Fig. 2 but with $\sigma_{2d} = -\sigma_{1d}$ and $X^d_{1\to 2} = 0.586\sigma_{2d}$ shown in (a) and (d). Stress values are -10 (yellow, light gray), 0 (green, intermediate gray), and 10 GPa (blue, dark gray). (b),(c) and (e),(f) are the intermediate and the stationary microstructures.

LANL and NSF (CMS-0555909) support and the help of A. Idesman with the FEAP code are acknowledged.

[1] A. Artemev, Y. M. Jin, and A. G. Khachaturyan, Acta Mater. **49**, 2309 (2001).
[2] L. Q. Chen, Annu. Rev. Mater. Res. **32**, 113 (2002).
[3] Y. U. Wang, Y. M. Jin, A. M. Cuitino, and A. G. Khachaturyan, Acta Mater. **49**, 1847 (2001).
[4] K. Ø. Rasmussen, T. Lookman, A. Saxena, A. R. Bishop, R. C. Albers, and S. R. Shenoy, Phys. Rev. Lett. **87**, 055704 (2001).
[5] A. E. Jacobs, S. H. Curnoe, and R. C. Desai, Phys. Rev. B **68**, 224104 (2003).
[6] W. C. Kerr, M. G. Killough, A. Saxena, J. Swart, and A. R. Bishop, Phase Transit. **69**, 247 (1999).
[7] S. Y. Hu, Y. L. Li, Y. X. Zheng, and L. Q. Chen, Int. J. Plast. **20**, 403 (2004).
[8] G. Ghosh and G. B. Olson, Acta Metall. Mater. **42**, 3361 (1994); M. Grujicic, G. B. Olson, and W. S. Owen, Metall. Trans. A **16**, 1713 (1985); V. I. Levitas, A. V. Idesman, G. B. Olson, and E. Stein, Philos. Mag. A **82**, 429 (2002).
[9] V. I. Levitas, A. V. Idesman, and D. L. Preston, Phys. Rev. Lett. **93**, 105701 (2004).
[10] V. I. Levitas and D. L. Preston, Phys. Rev. B **66**, 134206 (2002); V. I. Levitas, D. L. Preston, and D.-W. Lee, *ibid.* **68**, 134201 (2003).
[11] O. Zienkiewicz and R. Taylor, *The Finite Element Method* (Butterworth-Heinemann, Oxford, 2000), 5th ed.
[12] In [3], a periodic thermodynamic potential in terms of order parameters (''Peierls potential'') was introduced for dislocations. However, as shown in [7], it does not reproduce the Peierls barrier.